Dynamic Crossover of Critical Behavior in Polymer Blend Solutions

Naoshi Miyashita and Takuhei Nose*

Department of Polymer Chemistry, Tokyo Institute of Technology, Ookayama, Meguro-ku, Tokyo 152, Japan

Received June 30, 1995; Revised Manuscript Received October 30, 1995[⊗]

ABSTRACT: By the use of quasi-elastic light scattering, dynamic critical behavior was studied for symmetrical blend solutions of polystyrene/poly(methyl methacrylate)/deuterated benzene and polystyrene/poly(2-chlorostyrene)/deuterated benzene having different polymeric indices N and polymer concentrations c. The decay rate Γ_I of polymer-composition fluctuations showed the dynamic crossover from the diffusive to the mode−mode-coupled hydrodynamic behavior in all solutions. The dynamic-crossover number τ^*, which represents the distance between the stability limit and the location of the dynamic crossover, was comparable to that theoretically expected for the dynamically-unentangled system in the present ranges of N and c including a chain-entangled region. The blend solutions with entanglements exhibited a wider mode−mode-coupled regime than theoretical prediction. The dynamic-crossover number τ^* was larger than the Ginzburg number Gi, which characterizes the location of the static crossover from the mean-field to the nonclassical Ising behavior, and the mode−mode-coupled dynamics covered a wider region than the statical Ising behavior.

Introduction

Near the critical points of binary fluids, the static and dynamic crossovers occur with increasing amplitude of composition fluctuations. At the static crossover, the critical exponents of static properties change their values from those of the mean-field model into those of the three-dimensional Ising (3D Ising) model, while the dynamic one is the crossover in the fluctuation decay from the "diffusive" process to the "hydrodynamic" mode−mode-coupled process. Locations of the static and dynamic crossovers are characterized by the system-dependent parameters, the Ginzburg number Gi, and the dynamic-crossover number τ^*, respectively, which represent the temperature distance between the stability limit and the crossover.

Some theoretical[1−7] and experimental[8−13] studies on the static and dynamic crossovers have been done mainly for polymer blends. In polymeric systems, both crossover behaviors were observed more remarkably than small-molecular fluids, and Gi and τ^* are expected to depend upon the polymeric index N and/or the polymer concentration c. In bulk blend mixtures, however, experimental difficulties allow us to observe critical phenomena in a very limited N range only, so that a few discussions have been made on the scaling relation of Gi and τ^*, and their mutual relationship. In a previous work,[14] we investigated the static crossover for various polymer blend solutions with different N and c to determine the Belyakov−Kiselev-type Ginzburg number Gi^{BK} [15] and discussed the N and c dependence of Gi^{BK} by the use of the blob concept.[16−18] It has been revealed that the theoretically-predicted relation $Gi^{BK} \sim (N/g)^{-1}$ holds over the wide concentration range from the semidilute region to the bulk limit, where g is the segmental number per blob, being dependent on c. In this paper we are concerned with the dynamic crossover for polymer blend solutions, for which no experimental result has been reported to our knowledge.

Decay rates Γ of the critical fluctuation by the diffusive process and the mode−mode-coupled (hydrodynamic) process are related to the microscopic diffusive mobility M_D of a molecule and the macroscopic shear viscosity η_M, respectively, as follows.

$$\Gamma(\text{diffusive process}) \propto M_D$$

$$\Gamma(\text{mode−mode-coupled process}) \propto 1/\eta_M$$

Chain entanglements reduce both M_D and $1/\eta_M$.[19,20] But the reduction of $1/\eta_M$ is larger than that of M_D at larger N, so that the diffusion becomes a dominant factor rather than the hydrodynamic back-flow as N increases. According to the analyses of Graessley[21] and Takahashi et al.,[22] the polymer solution can be classified into five concentration regions with different chain static and dynamic behaviors, as shown in the c−molecular weight (M) diagram of Figure 1, which was experimentally determined from shear viscosity for polystyrene in toluene. The line labeled c^* in the figure indicates the statical overlap concentration as a function of M (or N). The vertical dotted line corresponds to the statical boundary concentration c^{**} between the semidilute and

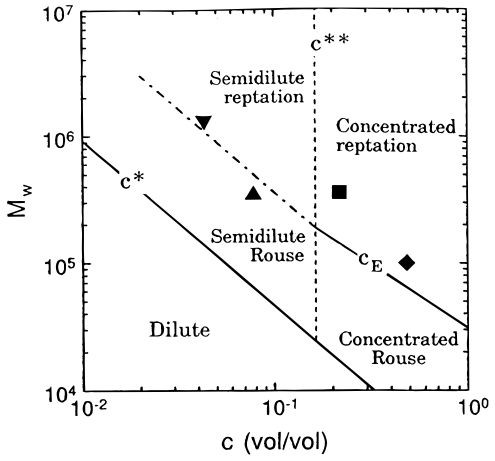

Figure 1. Molecular weight−concentration diagram of viscoleastic region for polystyrene in toluene, which was deduced from shear viscosity measurement by Takahashi et al.[22] Symbols represent the blend solutions used in this study: (▲) MA1a and MA1b; (▼) MA2; (♦) CL1; (■) CL2.

[⊗] Abstract published in *Advance ACS Abstracts,* January 1, 1996.

0024-9297/96/2229-0925$12.00/0

concentrated regions, which is independent of M. The line labeled c_E is the dynamical entanglement concentration. Solutions below c_E belong to the unentangled Rouse region, while the reptation model can be applied to those above c_E. In the reptation region, that is, a chain-entangled region, the dynamic-crossover number τ^* is expected to have c and N dependences different from those in the Rouse region.

In this study, by means of quasi-elastic light scattering (QELS), we have observed the dynamic critical phenomena for various polymer blend solutions and evaluated the dynamic crossover number τ^*. In the next section, the theoretical background of the dynamic crossover is reviewed, and the N and g dependences of τ^* in the Rouse and reptation regions are theoretically derived by the use of the blob concept. Then, experiments and data analyses are described, and the experimental results are compared with the theoretical scaling relation. Using the results of the previous paper,[14] we will also discuss the mutual relationship between the static and dynamic crossovers for blend solutions and bulk blends.

Theoretical Background

Critical Relaxation Equation for Fluids and the Dynamic Crossover. In fluid systems, the critical divergences of the isothermal susceptibility S_T and the fluctuation-correlation length ξ_t are respectively described as

$$S_T = S_{T0}\tau^{-\gamma} \tag{1}$$

$$\xi_t = \xi_{t0}\tau^{-\nu} \tag{2}$$

Here S_{T0} and ξ_{t0} are the critical amplitudes and τ is the reduced temperature defined as $\tau \equiv |T/T_S - 1|$, where T_S is the temperature at the stability limit. The critical exponents γ and ν have the values $\gamma = 1$ and $\nu = {}^1/_2$ in the mean-field region and have the values $\gamma = 1.24$ and $\nu = 0.63$ in the 3D Ising region.[23] According to the mode−mode-coupling theory and the dynamic renormalization-group theory,[24−29] the decay rate Γ of the order-parameter fluctuations near the stability limit is expressed as the following function of S_T, ξ_t, and length q of the scattering vector.

$$\Gamma = \Gamma_b + \Gamma_c \tag{3}$$

$$= \frac{M_D}{S_T}q^2[1 + (q\xi_t)^2] + \frac{k_BT}{6\pi\eta_M\xi_t^3}RK(q\xi_t)\left[1 + \left(\frac{q\xi_t}{2}\right)^2\right]^{x_\eta/2} \tag{4}$$

$$K(x) = \frac{3}{4}[1 + x^2 + (x^3 - x^{-1})\tan^{-1}x] \tag{5}$$

Here k_B is the Boltzmann constant, R is a universal constant of order of unity, and x_η is a universal critical exponent of shear viscosity η_M expected to have the value 0.050−0.065.[29] $K(x)$ is the so-called "Kawasaki function". The first term Γ_b and the second term Γ_c of the right-hand side of eq 3 describe the diffusive behavior and the mode−mode-coupled "hydrodynamic" behavior, respectively. Since Γ_b and Γ_c have different asymptotic forms at $q\xi_t < 1$ and $q\xi_t > 1$, the following characteristic regimes can be defined for the behavior of Γ, which are illustrated in Figure 2.

Regime A: $\xi_t < \xi^*$ and $q\xi_t < 1$ (diffusive). Fluctuation relaxation with the diffusive process. $\Gamma \sim \xi_t^{-2}q^2$.

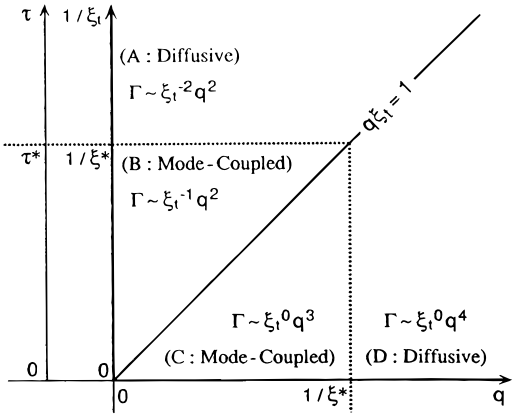

Figure 2. Schematic illustration of the observable regimes in QELS measurements near the stability limit for critical fluids or critical binary fluids.

Regime B: $\xi_t > \xi^*$ and $q\xi_t < 1$ (mode−mode-coupled). Fluctuation relaxation with the hydrodynamic backflow. $\Gamma \sim \xi_t^{-1}q^2$.

Regime C: $\xi_t > \xi^*$ and $q\xi_t > 1$ (mode−mode-coupled). Internal motions of fluctuations with the hydrodynamic interactions. $\Gamma \sim \xi_t^0q^3$.

Regime D: $\xi_t < \xi^*$ and $q\xi_t > 1$ (diffusive). Internal motions of fluctuations with no hydrodynamic interaction (diffusive). $\Gamma \sim \xi_t^0q^4$.

The classification of similar characteristic regimes was first made in the theoretical works by Fredrickson[5] for bulk blend mixtures. Here ξ^* is the dynamic-crossover correlation length which describes the boundary between the diffusive and the mode−mode-coupled regions and defined as the correlation length ξ_t at which the diffusive term Γ_b and the mode−mode-coupled term Γ_c have an equal contribution to Γ at the macroscopic limit ($q \to 0$).

$$\xi^* \equiv \lim_{q\to 0} \xi_t(\Gamma_b = \Gamma_c) \tag{6}$$

Similarly, we define the "dynamic-crossover number τ^*" as

$$\tau^* \equiv \lim_{q\to 0} \tau(\Gamma_b = \Gamma_c) \tag{7}$$

τ^* represents the distance between the stability limit and the dynamical crossover in the τ scale, being similar to the Ginzburg number Gi for the static crossover. The bare dynamic-crossover number τ^*(bare) evaluated by the mean-field approximation with bare interactions can be expressed, from eq 4, as below in terms of the bare (unrenormalized) amplitudes S_{T0}(bare) and ξ_{t0}(bare).

$$\tau^*(\text{bare}) = \left(\frac{k_BTRS_{T0}(\text{bare})}{6\pi\eta_M M_b\xi_{t0}(\text{bare})}\right)^2 \tag{8}$$

The Dynamic-Crossover Number τ^* for Polymer Blend Solutions with a Blob Model. Here, we will evaluate τ^*(bare) for a polymer A/polymer B/good solvent system with a blob picture in the framework of the mean-field theory to estimate the N and c dependence of the dynamic-crossover number τ^*. The blob model adopted here is the one used in the previous paper[14] for descriptions of the Ginzburg number Gi. First we will briefly review the previous results to explain the model and present expressions of S_{T0}(bare) and ξ_{t0}(bare). By the use of the blob concept,[16−18] the system is approximated by a quasi-binary mixture of Gaussian

chains of blobs. Here the bare critical amplitudes are defined as

$$S_{Tm} = S_{T0}(\text{bare})\, \tau_{\chi m}^{-1} \tag{9}$$

$$\xi_{tm} = \xi_{t0}(\text{bare})\, \tau_{\chi m}^{-1/2} \tag{10}$$

with the reduced interaction parameter τ_χ

$$\tau_\chi \equiv |1 - \frac{\chi_b}{\chi_{bs}}| \tag{11}$$

where χ_b is the Flory−Huggins interaction parameter per blob between unlike polymers and χ_{bs} is χ_b at the spinodal temperature T_S. The subscript "m" denotes the mean-field; i.e., $\tau_{\chi m}$ is the mean-field-type reduced interaction parameter defined as $\tau_{\chi m} \equiv |1 - \chi_b/\chi_{bsm}|$ with the mean-field spinodal interaction parameter χ_{bsm}. The basic assumption that the blob volume $v_b(c)$ is common for the two polymers is imposed. As a result, the segment number $g(c)$ within a blob can commonly be taken if a single segment volume v_s is defined for both polymers. They have the following relation.

$$v_b(c) = v_s g(c)/c \tag{12}$$

The polymeric index N_i and the radius $R_{gi}(c)$ of gyration of an i-polymer chain are defined as

$$N_i = v_i/v_s \tag{13}$$

$$R_{gi}(c) = \left(\frac{N_i}{g(c)}\right)^{1/2} v_b^{1/3}(c) \tag{14}$$

where v_i is the volume of an i-chain and $N_i/g(c)$ corresponds to the reduced polymeric index, that is, the number of blobs per chain. $g(c)$ has different dependences on the polymer concentration c in the statical semidilute region ($c^* < c < c^{**}$) and the concentrated region ($c^{**} < c < 1$). From the boundary condition that $g = 1$ in bulk (at $c = 1$) and the assumption that $g(c)$ smoothly changes at $c = c^{**}$, one can define $g(c)$ uniquely to be

$$g(c) = (c^{**})^{-3(2\sigma-1)/(3\sigma-1)} c^{-1/(3\sigma-1)} \qquad (c^* < c < c^{**}) \tag{15}$$

$$g(c) = c^{-2} \qquad (c^{**} < c < 1) \tag{16}$$

The results of the Flory−Huggins theory and the random phase approximations for binary polymer mixtures[8c,14,30] yield the bare critical amplitudes S_{T0}(bare) and ξ_{t0}(bare) for the present model as

$$S_{T0}(\text{bare}) = \frac{1}{k_B T}\left(\frac{1}{(N_A/g)\phi_A} + \frac{1}{(N_B/g)\phi_B}\right)^{-1} = \frac{1}{k_B T}\frac{\langle N\rangle \phi_A \phi_B}{g} \tag{17}$$

$$\xi_{t0}^{\,2}(\text{bare}) = \frac{\langle N\rangle \phi_A \phi_B}{3g}\left(\frac{R_{gA}^{\,2}(c)}{(N_A/g)\phi_A} + \frac{R_{gB}^{\,2}(c)}{(N_B/g)\phi_B}\right) = \frac{\langle R_g^{\,2}(c)\rangle}{3} \tag{18}$$

where ϕ_i is the volume fraction of polymer i in the total volume of polymers ($\phi_A + \phi_B = 1$). Assuming the incompressibility, one has the following expression of the mobility M_D, that is, the so-called "slow theory"[31,32] (see a note of ref 33),

$$M_D = \left(\frac{1}{\mu_A(N_A/g)\phi_A} + \frac{1}{\mu_B(N_B/g)\phi_B}\right)^{-1} = \frac{\langle\mu\rangle\langle N\rangle\phi_A\phi_B}{g} \tag{19}$$

where μ_i is the self-diffusional mobility for an i-polymer chain, and the averages are defined as follows.

$$\langle N\rangle = \frac{\phi_A^{-1} + \phi_B^{-1}}{N_A^{-1}\phi_A^{-1} + N_B^{-1}\phi_B^{-1}} \tag{20}$$

$$\langle R_g^{\,2}(c)\rangle = \frac{R_{gA}^{\,2}(c)N_A^{-1}\phi_A^{-1} + R_{gB}^{\,2}(c)N_B^{-1}\phi_B^{-1}}{N_A^{-1}\phi_A^{-1} + N_B^{-1}\phi_B^{-1}} \tag{21}$$

$$\langle\mu\rangle = \frac{N_A^{-1}\phi_A^{-1} + N_B^{-1}\phi_B^{-1}}{\mu_A^{-1}N_A^{-1}\phi_A^{-1} + \mu_B^{-1}N_B^{-1}\phi_B^{-1}} \tag{22}$$

Then, the bare dynamic-crossover number τ_χ^*(bare), which is the one defined by the interaction parameter χ_b, is evaluated by eq 8 with eqs 17−19 to be

$$\tau_\chi^*(\text{bare}) = \frac{3}{\langle R_g^{\,2}(c)\rangle}\left(\frac{R}{6\pi\eta_M\langle\mu\rangle}\right)^2 \tag{23}$$

The shear viscosity η_M and the self-diffusional mobility μ_i have the different g and N dependences in the Rouse and reptation regions, respectively.[19,20] Thus τ_χ^*(bare) also have the different g and N dependences in both dynamical regions.

(i) In the Rouse region, since μ_i is described as $\mu_i = (N_i/g)^{-1}\mu_{bi}$, $\langle\mu\rangle$ is rewritten as

$$\langle\mu\rangle = \left(\frac{\langle N\rangle}{g}\right)^{-1}\langle\mu_b\rangle \tag{24}$$

$$\langle\mu_b\rangle = \frac{\phi_A^{-1} + \phi_B^{-1}}{\mu_{bA}^{-1}\phi_A^{-1} + \mu_{bB}^{-1}\phi_B^{-1}} \tag{25}$$

where μ_{bi} is the self-diffusional mobility per blob of an i-polymer. The macroscopic shear viscosity η_M is assumed to be expressed as follows in terms of v_b and the averages[19]

$$\eta_M = \frac{1}{6}v_b^{-1/3}\langle\mu_b\rangle^{-1}\left(\frac{\langle N\rangle}{g}\right) \tag{26}$$

Using eqs 14, 24, and 26, one can rewrite eq 23 to obtain the expression of τ_χ^*(bare)

$$\tau_\chi^*(\text{bare,Rouse}) = \frac{3R^2}{\pi^2}\left(\frac{\langle N\rangle}{g}\right)^{-1} \tag{27}$$

τ_χ^*(bare, Rouse) has the $\langle N\rangle^{-1}$ dependence in both the semidilute and concentrated c ranges, so that if a scaled dynamic-crossover number t_χ^* is defined as

$$t_\chi^* \equiv \tau_\chi^*\langle N\rangle \tag{28}$$

then the scaled bare dynamic-crossover number t_χ^*(bare, Rouse) can be expressed as

$$t_\chi^*(\text{bare,Rouse}) = \frac{3R^2}{\pi^2}g(c) \tag{29}$$

t_χ^*(bare) in the Rouse region is a function of g(c), that is, a function of c alone, over the semidilute and the

concentrated regions. It is noteworthy that τ_χ*(bare,Rouse) is proportional to the bare Ginzburg number G_i^{BK}(bare) and they have the following relations.

$$\tau_\chi^*(\text{bare,Rouse}) = \frac{8\pi^2 R^2}{9} f_\phi^{-1} Gi^{BK}(\text{bare}) \quad (30)$$

$$f_\phi = \phi_A^2 \phi_B^2 \left(\frac{N_A^{-1}\phi_A^{-3} + N_B^{-1}\phi_B^{-3}}{N_A^{-1}\phi_A^{-1} + N_B^{-1}\phi_B^{-1}} \right)^2 \quad (31)$$

Here f_ϕ is the asymmetry factor for the composition. When $\phi_A = \phi_B = {}^1/_2$, f_ϕ becomes unity and eq 30 is reduced to τ_χ*(bare,Rouse) $\approx (8-12)Gi^{BK}$(bare) for $R = 1-1.2$.

Roby and Joanny[6] had also discussed the composition relaxation for the symmetrical unentangled blend solutions, i.e., $N_A = N_B = N$ and $\phi_A = \phi_B = {}^1/_2$, by taking into account the hydrodynamic interaction through the Oseen tensor. They derived the following expression for ξ* in the Rouse region.

$$\frac{\nu_b^{1/3}(c)}{\xi^*} \sim \frac{\eta_0}{\eta_M} \quad \text{(Rouse region)} \quad (32)$$

Here η_0 is the solvent viscosity. Equation 32 is consistent with eqs 10 and 27 except for the numerical prefactors.

(ii) In the reptation region, if it is assumed that $\langle N \rangle$ is a continuous variable and $\langle \mu \rangle$ and η_M smoothly change from the Rouse behavior to the reptation behavior at $c = c_E$, $\langle \mu \rangle$ and η_M can be expressed as the following functions of $\langle N \rangle$ and g.

$$\langle \mu \rangle = \left(\frac{\langle N \rangle}{g_E} \right) \left(\frac{\langle N \rangle}{g} \right)^{-2} \langle \mu_b \rangle \quad (33)$$

$$\eta_M = \frac{1}{6} \nu_b^{-1/3} \langle \mu_b \rangle^{-1} \left(\frac{\langle N \rangle}{g_E} \right)^{-2} \left(\frac{\langle N \rangle}{g} \right)^3 \quad (34)$$

Here g_E is g at the entanglement concentration c_E shown in Figure 1, which follows $g_E \sim c_E^{-1/(3\sigma-1)} \sim N$ for $c^* < c_E < c^{**}$ and $g_E \sim c_E^{-2} \sim N^2$ for $c^{**} < c_E < 1$. From these equations, the g and N dependence of τ_χ*(bare) is derived to be

$$\tau_\chi^*(\text{bare,reptation}) = \frac{3R^2}{\pi^2} \left(\frac{\langle N \rangle}{g_E} \right)^2 \left(\frac{\langle N \rangle}{g} \right)^{-3} \quad (35)$$

$$= \frac{3R^2}{\pi^2} \langle N \rangle^{-1} g^3 g_E^{-2} \quad (36)$$

τ_χ*(bare,reptation) is not proportional to Gi^{BK}(bare), and the universality of the scaled dynamic-crossover number t_χ*(bare), similar to eq 29, fails, because g_E depends on N.

Experimental Section

Materials. Weight-average molecular weight M_W and polydispersity index M_w/M_n are listed in Table 1 for polystyrene (PS), poly(methyl methacrylate) (PMMA), and poly(2-chlorostyrene) (P2ClS), along with material codes and sources. Numbers in the material codes refer to the molecular weight in 10 kg/mol.

Samples. Blend solutions used were PS/PMMA/deuterated benzene (Bnz-d_6) solutions and PS/P2ClS/Bnz-d_6 solutions, all of which had the lower critical solution temperature. Two polymer components in respective blend solutions had approximately the same molecular weight, and Bnz-d_6 was thermodynamically good for all of PS, PMMA, and P2ClS. Details of sample preparation were described in the previous paper.[14] Sample codes and characteristics of the blend solutions are listed in Table 2. Polymer compositions (ϕ_{PS}) of the samples MA1b, MA2, CL1, and CL2 were close to the critical compositions that were predicted by the Flory−Huggins theory[30] for bulk polymer blends corresponding to respective blend solutions. Although the solutions might not be real critical ones, they could reach temperatures sufficiently close to the stability limit with no phase separation. The values of $\langle N \rangle$, $\langle N \rangle/g$, and the blob size $\nu_b^{1/3}(c)$ were calculated from the segmental volume ν_s, which was determined on the basis of the unperturbed radius $R_{g\theta}$ and the density of a PS chain.[14] M_w and total polymer concentration c of blend solutions are also shown in Figure 1. The values of c_E in the figure are given by the following expressions, which were determined for PS from viscoelastic experiments[21,22]

$$c_E = 1.77 \times 10^3 M_w^{-0.764} \quad (c^* < c_E < c^{**}) \quad (37)$$

$$c_E = 3.1 \times 10^4 M_w^{-1} \quad (c^{**} < c_E < 1) \quad (38)$$

According to this map, the samples extend over three regions, that is, the semidilute Rouse region, the semidilute reptation region, and the concentrated reptation region.

Table 1. Weight-Average Molecular Weight and Polydispersity Index of the Polymers Used in This Study

material code	$10^{-5}M_w$	M_w/M_n	note
polystyrene			
PS10	10.0	≤1.06	a product of Pressure Chemicals
PS36	35.5	1.02	a product of Tosoh
PS126	126	1.05	a product of Tosoh
poly(methyl methacrylate)			
PMMA33	32.7	≤1.10	a product of Pressure Chemicals
PMMA109	109	1.08	radical-polymerized
poly(2-chlorostyrene)			
P2ClS12	12.4	1.19	radical-polymerized
P2ClS37	36.9	1.23	radical-polymerized

Quasi-Elastic Light Scattering. The optical system was a specially designed one, where an Ar ion laser operated at 488 nm was used as a light source and the scattered light was detected by a photomultiplier tube Hamamatsu Photonics R464. A sample tube of 4.2 nm inner diameter was immersed in a thermostated (±0.05 °C) index-matching oil bath. Photoelectron-counted autocorrelation function $G^{(2)}(q,t)$ was measured in the angular range $20° \le \theta \le 130°$ with an ALV-5000 multiple τ digital correlator (288 channel) or a Kowa digital correlator Z-216 (64 channel). For the most concentrated solution CL1, the photoelectron-count-rate trace exhibited a large degree of nonergodicity in the smaller angular range $\theta \le 50°$ ($q \le 1.641 \times 10^{-2}$ nm^{-1}), as shown in Figure 3a. This probably arises from the presence of composition inhomogeneity which was hardly quenched because of high viscosity of the solution. In static light scattering experiments, enhancement of scattered light intensity was also observed in the same angular range.[14] Thus, for the CL1 solution, we had evaluated $G^{(2)}(q,t)$ only in the higher angular range of $\theta \ge 60°$ ($q \ge 1.941 \times 10^{-2}$ nm^{-1}) where the count-rate trace was ergodic (Figure 3b). No correction for the turbidity attenuation and multiple scattering effects was made for the measured $G^{(2)}(q,t)$, since the Rayleigh ratio of the scattered light intensity had been hardly influenced by them in the static measurements at the same temperature ranges as in the present cases.[14]

The scattering function $S(q,t)$ can be related to $G^{(2)}(q,t)$ by the Siegelt relation:[34]

$$G^{(2)}(q,t) = A[1 + \beta |S(q,t)|^2] \quad (39)$$

Here A and β are constants. In a symmetrical polymer A/polymer B/good solvent system, $S(q,t)$ has two decay modes at least, that is, the cooperative diffusion mode of fluctuations in total polymer concentration c and the interdiffusive mode of polymer-composition fluctuations. For the blend solutions

Table 2. Characteristics of Polymer Blend Solutions

sample code	system	ϕ_{PS}	c/vol % (c/c^*)[a]	$\langle N\rangle$[b]	$\langle N\rangle/g$[b]	$v_b^{1/3}$/nm[b]	T_s/K[c]
MA1a	PS36/PMMA33/Bnz-d_6	0.249	8.16 (8.89)	75.8	2.00	14.8	335.9
MA1b		0.526	8.30 (9.04)	75.8	2.00	14.8	299.2
MA2	PS126/PMMA109/Bnz-d_6	0.497	4.33 (12.7)	259	3.02	24.1	320.6
CL1	PS10/P2ClS12/Bnz-d_6	0.469	48.9 (19.7)	17.5	4.48	4.3	334.7
CL2	PS36/P2ClS37/Bnz-d_6	0.452	21.8 (23.8)	58.7	5.38	7.8	330.5

[a] The values of c/c^* were calculated with the swelling radius R_F in a good solvent and the molecular weight M_w for a PS chain.[14] [b] Calculated from the common segmental volume v_s which is determined on the basis of the unperturbed radius $R_{g\theta}$ and the density of a PS chain.[14] [c] Estimated in the static light scattering measurement.[14]

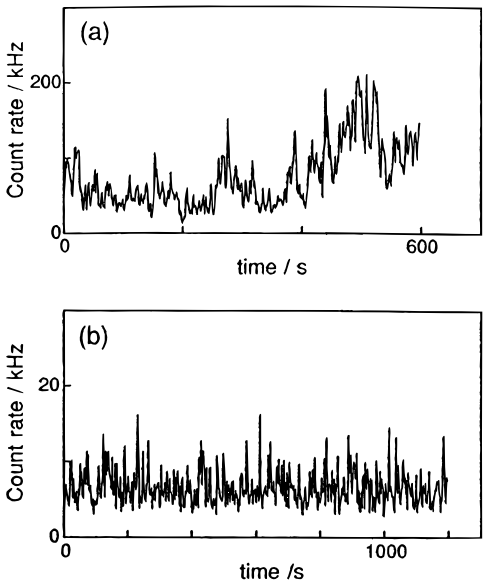

Figure 3. Time change of the scattered intensity measured by QELS measurements for the CL1 blend solution. (a) A nonergodic pattern measured at $q = 6.741 \times 10^{-3}$ nm^{-1} ($\theta = 20°$). (b) An ergodic pattern measured at $q = 1.941 \times 10^{-2}$ nm^{-1} ($\theta = 60°$).

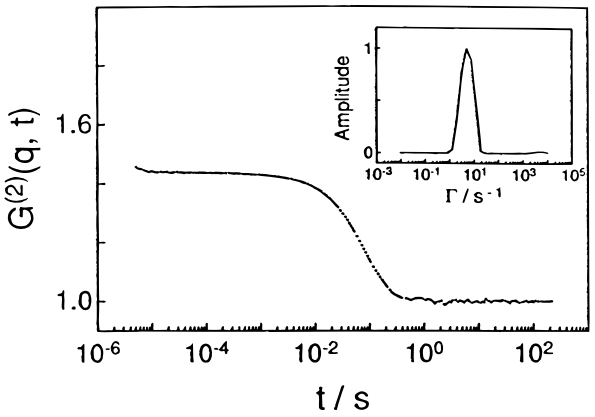

Figure 4. Typical autocorrelation function $G^{(2)}(q,t)$ of the scattered light intensity measured by QELS on MA2 solution at $q = 6.741 \times 10^{-3}$ nm^{-1} ($\theta = 20°$) and $T = 283.3$ K. The inset represents the decay rate distribution obtained from the Laplace inversion routine CONTIN.

used in this study, most of scattering light intensity comes from polymer-composition fluctuations[14] and the experimental $G^{(2)}(q,t)$ showed a single exponential decay, though the distribution of the decay rate was slightly large (see Figure 4). The cooperative decay rate Γ_{coop} is expected from the relation[6,7] $\Gamma_{coop} \approx (k_B T/6\pi\eta_0 v_b^{1/3}(c))\, q^2$ to be 10^3–10^5 s^{-1} for the present case and is much larger than the decay rate observed here. Therefore we identified it as the interdiffusive decay rate Γ_I and evaluated Γ_I values by the use of the cumulant method.

Shear Viscosity. Shear viscosity was estimated for solutions MA1a, MA1b, MA2, and CL2 by the following semiexperimental equation, eq 40, because of experimental difficulties in homogenization of polymer composition inside the used viscometer. The shear viscosity η_M for a polymer A/polymer B/solvent C system at a fixed total polymer concentration has the following relation, which has been experimentally confirmed in the previous work.[35]

$$\eta_M(\phi_A,T) = \phi_A\eta_A(T) + (1-\phi_A)\eta_B(T) \tag{40}$$

Here ϕ_A is the volume fraction of polymer A in the total volume of polymers, and η_A and η_B are the shear viscosity of polymer A/solvent C and polymer B/solvent C solutions, respectively. The values of η_A and η_B for each blend solution were measured by using a rolling-ball type viscometer consisting of a glass capillary tube (1.8 mm inner diameter) and a bearing steel ball (1.2 mm diameter, density = 7.72 g cm^{-3}).[35] η_A and η_B exhibited no dependence on the shear rate in the present experimental conditions. The temperature dependence of η_M was described with the following Arrhenius equation

$$\eta_M = A_\eta \exp(B_\eta/k_B T) \tag{41}$$

where A_η and B_η are constants. The values of A_η and B_η obtained by fitting the data to eq 41, along with the value of η_M at the spinodal temperature T_S, are listed in Table 3. Figure 5 represents the temperature dependence of η_M for MA1b, MA2, and CL2 solutions.

For the most concentrated solution CL1, shear viscosity η_M was estimated to be much larger than 50 poise around 300 K[36] and could not be quantitatively evaluated by the above procedure. Therefore only the activation-energy parameter B_η was evaluated from the self-diffusion of hydrogenated benzene (Bnz-h_6) in the PS/P2ClS/Bnz-h_6 solution with the same M_W and c as CL1.[37–39] The self-diffusion coefficient D_S was measured by the pulsed-field-gradient nuclear magnetic resonance (PFG-NMR) method. Equipment and data analysis of PFG-NMR have been described in detail in the previous paper.[35] The measurement was performed by magnetic-field-gradient pulses of magnitude 379.8 G cm^{-1}, duration up to 5 ms and interval 50 ms.

Table 3. Shear Viscosity and Dynamic Critical Properties and of Polymer Blend Solutions

sample code	$\eta_M(T_s)$/ poise[a]	$10^3 A_\eta$/ poise	$10^{13} B_\eta$/ erg	ξ^*/nm	τ_χ^*	t_χ^*
MA1a	0.24	1.61	2.31	16.5	0.605	45.9
MA1b	0.50	1.62	2.36			
MA2	0.62	3.17	2.34	114	0.097	36.4
CL1	>20[b]		3.62[c]	4–14	0.2–0.6	3–10
CL2	6.41	4.16	4.16	42.2	0.128	7.5

[a] The shear viscosity at the spinodal temperature T_s for each blend solution. [b] A rough estimate calculated on the basis of the published data.[36] [c] Estimated from the temperature dependence of the self-diffusion coefficient D_s of hydrogenated benzene in the PS/P2ClS/hydrogenated benzene system with the same M_w and c as the CL1 solution.[37–39]

Results and Discussion

***q* and ξ_t Dependence of Γ_I.** The q dependence of Γ_I for MA1b, MA2, and CL2 solutions at different temperatures is shown in Figure 6 as double-logarithmic plots

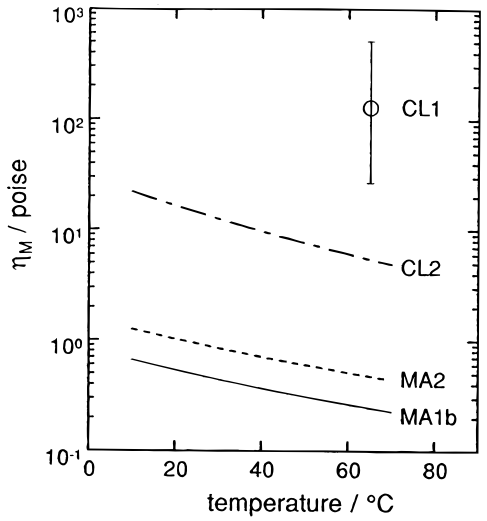

Figure 5. Temperature dependence of the shear viscosity η_M for the polymer blend solutions, MA1b, MA2, and CL2, which were estimated from eq 40 and shear viscosity for pure polymer solutions. The symbol (○) with an error bar represents the rough estimate of η_M for solution CL1 at $T = 280-350$ K, which was calculated on the basis of the published data.[36]

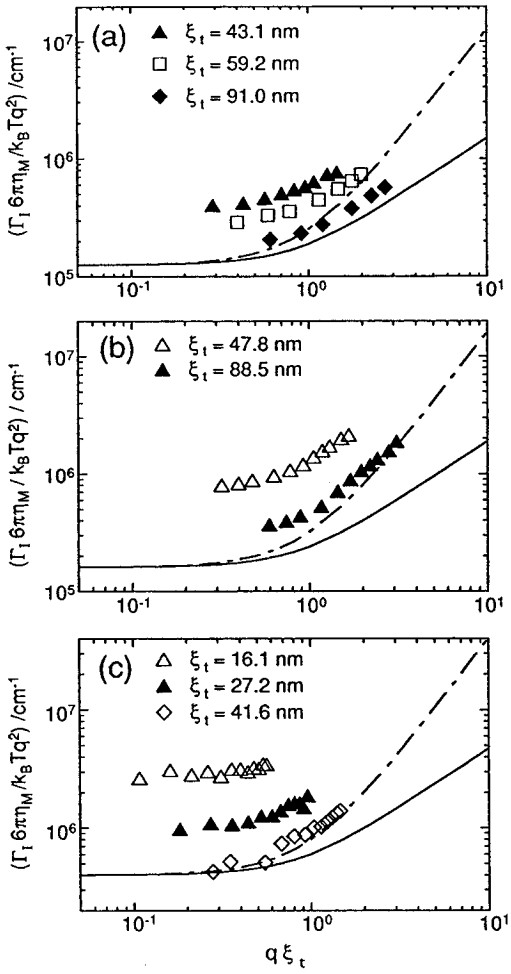

Figure 6. Double-logarithmic plots of the reduced decay rate $\Gamma_I 6\pi\eta_M/k_BTq^2$ vs $q\xi_t$ at fixed correlation length ξ_t for various blend solutions: (a) MA1b; (b) MA2; (c) CL2. Solid and broken lines represent the mode−mode-coupled term Γ_c and the diffusive term Γ_b in arbitrary scales, respectively.

of $\Gamma_I 6\pi\eta_M/k_BTq^2$ vs $q\xi_t$. Data of the correlation length ξ_t were obtained from static light scattering measurements.[14] Broken and solid lines in the figure represent

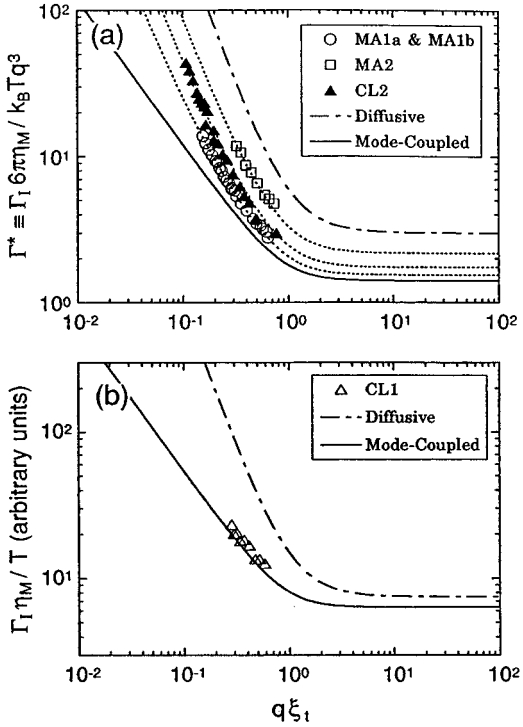

Figure 7. ξ_t dependence of the decay rate Γ_I measured at fixed length q of the scattering vector. (a) The scaled decay rate $\Gamma^* \equiv \Gamma_I 6\pi\eta_M/k_BTq^3$ measured at $q = 6.741 \times 10^{-3}$ nm^{-1} ($\theta = 20°$) for MA1b, MA2, and CL2 solutions. The data for MA1b contain those for MA1a with the same M_w and c. The broken line represents the diffusive term Γ_b in arbitrary scales, and the solid line represents the mode−mode-coupled term Γ_c calculated with $R = 1.20$ and $x_\eta = 0$.[35] Dotted lines indicate the results of fitting to eq 43. (b) The reduced decay rate $\Gamma_I\eta_M/T$ in arbitrary scales measured at $q = 1.941 \times 10^{-2}$ nm^{-1} ($\theta = 60°$) for CL1 solution. Broken and solid lines represent Γ_b and Γ_c in arbitrary scales, respectively.

the diffusive term Γ_b and the mode−mode-coupled term Γ_c in eq 4, respectively, in arbitrary scales. The plots for MA1b exhibit a gradual change from the $\Gamma_I \sim q^2$ behavior to the $\Gamma_I \sim q^3$ behavior around $q\xi_t = 1$, which may correspond to a change from regime B to regime C within the mode−mode-coupled regime. On the contrary, the data for MA2 and CL2 solutions apparently show a higher slope than the $\Gamma_I \sim q^3$ behavior (the solid lines) in the region of $q\xi_t \geq 1$. This suggests that the observed ranges of dynamics for MA2 and CL2 are located at regions closer to the diffusive regime (regime D) than those of MA1b.

Figure 7a shows the ξ_t dependence of Γ_I at $q = 6.741 \times 10^{-3}$ nm^{-1} ($\theta = 20°$) for MA1a, MA1b, MA2, and CL2 solutions in the double-logarithmic plots of the scaled decay rate $\Gamma^* \equiv \Gamma_I 6\pi\eta_M/k_BTq^3$ vs $q\xi_t$. It should be noted that plots for both MA1a and MA1b are on a single curve, where MA1a and MA1b have the same M_w and c, but different polymer compositions ϕ_{PS}. Broken lines in the figure represent the theoretical behavior of the diffusive term Γ_b in arbitrary scales. The theoretical values of the mode−mode-coupled term Γ_c are represented in quantitative scales by solid lines, which were calculated by eq 4 with $R = 1.20$ and $x_\eta = 0$. In the previous paper,[35] we have demonstrated that the value of $R = 1.20$ gives a better agreement with the result of a symmetrical blend solution than $R = 1.00$ or 1.03. Deviation of the plots from the solid line shows the presence of diffusive term Γ_b, and the larger deviation indicates the larger Γ_b. Solutions with larger deviations show the ξ_t dependence closer to the diffusive behavior,

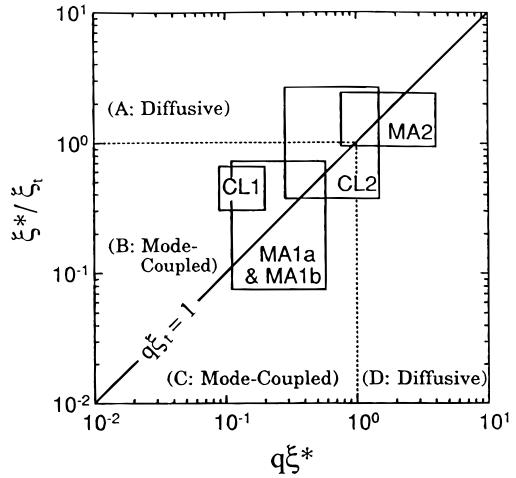

Figure 8. Double-logarithmic plots of the reduced correlation length ξ^*/ξ_t vs the reduced length $q\xi^*$ of the scattering vector. The rectangles represent the regimes experimentally studied in this work.

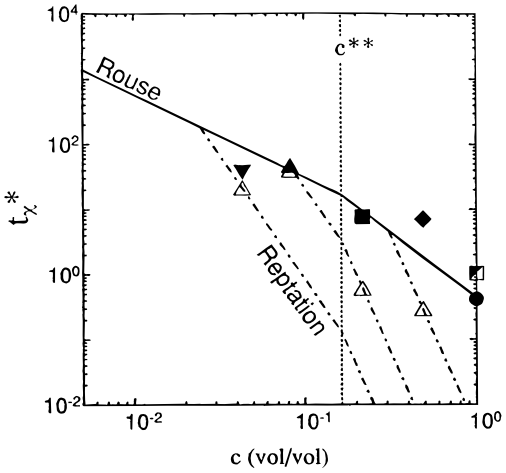

Figure 9. Double-logarithmic plots of the scaled dynamic-crossover number $t_\chi^* \equiv \tau_\chi^*\langle N\rangle$ vs c. The symbols (▲, ▼, ♦, and ■) are the same as in Figure 1. Solid and broken lines represent the bare dynamic crossover number τ_χ^*(bare) in the Rouse (eq 27) and reptation regions (eq 35), respectively, which are calculated with $R = 1.20$ and the values of c^{**} and c_E shown in Figure 1. The values of τ_χ^*(bare) for each blend solution are indicated by the symbol △. Other symbols: (●) a polyisoprene/poly(ethylenepropylene) blend (Stepanek et al.[11]); (◩) a poly(dimethylsiloxane)/poly(ethylmethylsiloxane) blend (Meier et al.[12]).

$\Gamma_I \sim \xi_t^{-2}$ in the region of $q\xi_t < 1$. In Figure 7b is shown the ξ_t dependence of Γ_I measured at $q = 1.941 \times 10^{-2}$ nm^{-1} ($\theta = 60°$) for CL1, along with Γ_b and Γ_c drawn in arbitrary scales. The data exhibited the mode−mode-coupled behavior; nevertheless CL1 is the most dense and viscous system.

Scaling Analysis of the Dynamic-Crossover Number τ_χ^*. For MA1b, MA2, and CL2 solutions, we have estimated the dynamic-crossover correlation length ξ^* by fitting the data to the following equations.

$$\Gamma = \Gamma_b^{exp} + \Gamma_c \tag{42}$$

$$= A_G \frac{k_B T}{\eta_M \xi_t^2} q^2[1 + (q\xi_t)^2] + \frac{k_B T}{5\pi\eta_M \xi_t^3} K(q\xi_t) \tag{43}$$

This is equivalent to eq 4 with $R = 1.20$, $\chi_\eta = 0$, but Γ_b^{exp} is an experimentally-determinable form of Γ_b with A_G being a fitting parameter. The fitting curves are shown by dotted lines in Figure 7a. The value of ξ^* was obtained from the condition $\Gamma_b^{exp} = \Gamma_c$. The dynamic-crossover number τ_χ^* can be evaluated from the temperature T^* at which $\xi_t = \xi^*$ using the temperature dependence of χ_b, which was determined through analysis of static critical behavior in the previous paper.[14] The obtained values of ξ^*, τ_χ^*, and the scaled dynamic-crossover number $t_\chi^* \equiv \tau_\chi^*\langle N\rangle$ are listed in Table 3. Here, for CL1, a possible range of the τ_χ^* value was indicated in the table. The range of τ_χ^* was determined from the fact that ξ^* should be larger than the blob size $v_b^{1/3}(c)$, while ξ^* had to be smaller than the experimental ξ_t range where the mode−mode-coupled behavior was observed. Using the obtained ξ^*, the experimentally-studied regimes are illustrated on the dynamical map of Figure 8 similar to Figure 2. MA1a, MA1b, and CL1 are located in the mode−mode-coupled regime, MA2 is in the diffusive regime, and CL2 is on the boundary between these regimes.

Figure 9 shows the concentration dependence of the experimental value of τ_χ^* for MA1a + MA1b, MA2, CL1, and CL2 solutions in the double-logarithmic plots of the scaled dynamic-crossover number $t_\chi^* \equiv \tau_\chi^*\langle N\rangle$ vs c. Reported results for unentangled symmetrical polymer bulk blends[11,12] are also plotted at $c = 1$. Solid and broken lines represent the bare dynamic-crossover number τ_χ^*(bare) in the Rouse (eq 27) and reptation regions (eq 35), respectively, which are calculated with $R = 1.20$ and the values of c^{**} and c_E shown in Figure 1. Filled points indicate the experimental values, while hollow points indicate the predicted bare ones. CL1 and CL2 solutions, which belong to the concentrated reptation region in Figure 1, have a much smaller value of t_χ^*(bare) than t_χ^*(bare,Rouse). But their experimental values t_χ^* are rather consistent with t_χ^*(bare,Rouse), so that t_χ^* values for all blend solutions exhibit a gradual decrease with increasing polymer concentration c. This may suggest that a polymer concentration much higher than c_E in Figure 1 is needed to enhance the diffusive mode in critical dynamics of blend solutions. In other words, the critical dynamics in blend solutions and blends is not so much influenced by the chain entanglement as the shear viscosity of pure polymer solutions and pure polymer melts. It was reported by Brown et al.[41] that the entanglement is inhibited due to incompatibility in PS/polyisobutylene/benzene solutions. This may be able to explain the present results. We can also point out that the value of c_E depends on the dynamic properties in general.

Relation between τ_χ^* and *Gi*. Figure 10 shows comparison of the c dependence of the scaled Ginzburg number $gi^{BK} \equiv Gi^{BK}\langle N\rangle f_\phi^{-1}$ and the scaled dynamic-crossover number $t_\chi^* \equiv \tau_\chi^*\langle N\rangle$ for blend solutions. The gi^{BK} values were evaluated in the previous paper.[14] Typical values of gi^{BK} and t_χ^* reported for bulk polymer blends[8,9,11,12] were also plotted at $c = 1$ in the figure. All systems for which both static- and dynamic-crossover behaviors have been so far studied are unentangled systems from the viewpoint of dynamic critical behavior. Hence, as expected in the mean-field treatment (eq 30), which predicts that the value of t_χ^* is larger than gi^{BK}, the dynamical mode−mode-coupled behavior covers a wider region than the statical 3D Ising behavior, and this mutual relationship between gi^{BK} and t_χ^* shows no characteristic change over the concentration range from the semidilute region to the bulk limit. In the reptation region, however, the decrease of t_χ^*-(bare) is stronger than that of gi^{BK}(bare) (eq 35), so that

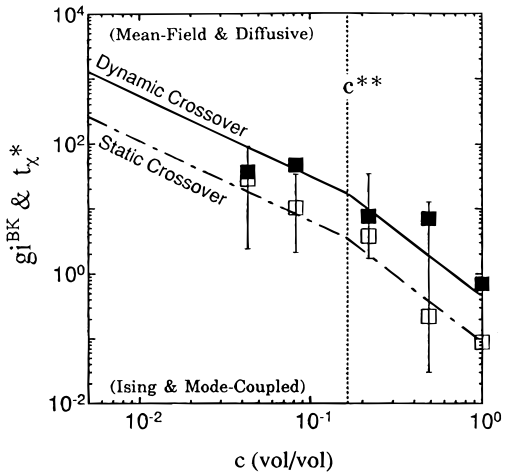

Figure 10. Concentration dependence of the scaled Ginzburg number $gi^{BK} \equiv Gi^{BK}\langle N\rangle f_\phi^{-1}$ and the scaled dynamic-crossover number $t_\chi^* \equiv \tau_\chi^*\langle N\rangle$ for polymer blend solutions. The symbols (□ and ■) represent gi^{BK} and t_χ*, respectively. Symbols at $c = 1$ correspond to the typical values of the reported data for polymer blends.[8,9,11,12] Vertical lines correspond to the regime experimentally studied in the previous paper[14] and this work. Solid and broken lines superposed upon symbols, which are guides for the eye, have the same slope as the polymeric index $g(c)$ within a blob.

one might see the intersection of the gi^{BK} and t_χ* curves in blend solutions with much larger M and c, or in bulk blends with larger M.

References and Notes

(1) de Gennes, P. G. *J. Phys. Lett.* **1977**, *38*, L-411.
(2) Joanny, J. F. *J. Phys. A.: Math. Gen.* **1978**, *11*, L-117.
(3) (a) Dudowicz, J.; Lifschitz, M.; Freed, K. F.; Douglas, J. F. *J. Chem. Phys.* **1993**, *99*, 4804. (b) Lifschitz, M.; Dudowicz, J.; Freed, K. F. *J. Chem. Phys.* **1994**, *100*, 3957.
(4) Holyst, R.; Vilgis, T. A. *J. Chem. Phys.* **1993**, *99*, 4835.
(5) Fredrickson, G. H. *J. Chem. Phys.* **1986**, *85*, 3556.
(6) Roby, F.; Joanny, J. F. *Macromolecules* **1992**, *25*, 4612.
(7) Benmouna, M.; Seils, J.; Meier, G.; Patokowski, A.; Fischer, E. W. *Macromolecules* **1993**, *26*, 668.
(8) (a) Schwahn, D.; Mortensen, K.; Yee-Maderia, H. *Phys. Rev. Lett.* **1987**, *58*, 1544. (b) Schwahn, D.; Mortensen, K.; Springer, T.; Yee-Maderia, H.; Thomas, R. *J. Chem. Phys.* **1987**, *87*, 6708. (c) Schwahn, D.; Janssen, S.; Springer, T. *J. Chem. Phys.* **1992**, *97*, 8775. (d) Meier, G.; Schwahn, D.; Mortensen, K.; Janssen, S. *Europhys. Lett.* **1993**, *22*, 577. (e) Schwahn, D.; Meier, G.; Mortensen, K.; Janssen, S. *J. Phys. II Fr.* **1994**, *4*, 837.
(9) Bates, F. S.; Rosedale, J. H.; Stepanek, P.; Lodge, T. P.; Wiltzius, P.; Fredrickson, G. H.; Hjelm, R. P., Jr. *Phys. Rev. Lett.* **1990**, *65*, 1893.
(10) (a) Chu, B.; Ying, Q.; Linliu, K.; Xie, P.; Gao, T.; Li, Y.; Nose, T.; Okada, M. *Macromolecules* **1992**, *25*, 7382. (b) Kwak, K. D.; Okada, M.; Chiba, T.; Nose, T. *Macromolecules* **1992**, *25*, 7204.
(11) Stepanek, P.; Lodge, T. P.; Kedrowski, C.; Bates, F. S. *J. Chem. Phys.* **1991**, *94*, 8289.
(12) Meier, G.; Momper, B.; Fischer, E. W. *J. Chem. Phys.* **1992**, *97*, 5884.
(13) Yajima, H.; Hair, D. W.; Nakatani, A. I.; Douglas, J. F.; Han, C. C. *Phys. Rev. B* **1993**, *47*, 12268.
(14) Miyashita, N.; Nose, T. *Macromolecules* **1995**, *28*, 4433.
(15) (a) Anisimov, M. A.; Kiselev, S. B.; Sengers, J. V.; Tang, S. *Physica A* **1992**, *188*, 487. (b) Belyakov, M. Y.; Kiselev, S. B. *Physica A* **1992**, *190*, 75.
(16) de Gennes, P.-G. *Scaling Concepts in Polymer Physics*; Cornell Univerity Press: Ithaca, NY, 1979.
(17) Daoud, M.; Jannnik, G. *J. Phys. (Paris)* **1976**, *37*, 973.
(18) Nose, T. *J. Phys.* **1986**, *47*, 517.
(19) Doi, M.; Edwards, S. F. *The Theory of Polymer Dynamics*; Clarendon Press: Oxford, U.K., 1990.
(20) Lodge, T. P.; Rotstein, N. A.; Prager, S. *Adv. Chem. Phys.* **1990**, *79*, 1.
(21) Graessley, W. W. *Polymer* **1980**, *21*, 258.
(22) (a) Takahashi, Y.; Isono, Y.; Noda, I.; Nagasawa, M. *Macromolecules* **1985**, *18*, 1002. (b) Noda, I. *Molecular Conformation and Dynamics of Macromolecules in Condensed Systems*; Nagasawa, N., Ed.; Elsevier: Amsterdam, 1988.
(23) Anisimov, M. A.; Kiselev, S. B. *Sov. Tech. Rev. Sec. B Therm. Phys.* **1992**, *3* (2), 1.
(24) Kadanoff, L.; Swift, J. *Phys. Rev.* **1968**, *166*, 89.
(25) Kawasaki, K. *Ann. Phys. (NY)* **1970**, *61*, 1.
(26) Oxtoby, D. W.; Gelbart, W. M. *J. Chem. Phys.* **1974**, *61*, 2957.
(27) (a) Kawasaki, K.; Lo, S. M. *Phys. Rev. Lett.* **1972**, *29*, 48. (b) Ohta, T.; Kawasaki, K. *Prog. Theor. Phys.* **1976**, *55*, 1384.
(28) (a) Hohenberg, P. C.; Halperin, B. I. *Rev. Mod. Phys.* **1977**, *49*, 435. (b) Siggia, E. D.; Halperin, B. I.; Hohenberg, P. C. *Phys. Rev. B* **1976**, *13*, 2110.
(29) (a) Burstyn, H. C.; Sengers, J. V.; Bhattacharjee, J. K.; Ferrell, R. A. *Phys. Rev. A* **1983**, *28*, 1567. (b) Bhattacharjee, J. K.; Ferrell, R. A. *Phys. Rev. A* **1983**, *28*, 2362. (c) Sengers, J. V. *Int. J. Thermophys.* **1985**, *6*, 203.
(30) Flory, P. J. *Principles of Polymer Chemistry*; Cornell University Press: Ithaca, NY, 1953.
(31) de Gennes, P. G. *J. Chem. Phys.* **1980**, *72*, 4756.
(32) Brochard, F.; Jouffroy, J.; Levinson, P. *J. Phys. Lett.* **1983**, *44*, L-455.
(33) Equation 19 is referred to as the slow theory, while the fast theory gives

$$M_D = \phi_A^2 \phi_B^2 \left(\frac{\mu_A(N_A/g)}{\phi_A} + \frac{\mu_B(N_B/g)}{\phi_B} \right)$$

which has been derived by Kramer et al. (*Polymer* **1984**, *25*, 473). It had not become apparent which is more suited for the real system, the slow or fast theory. But, under the symmetrical condition, i.e., $N_A = N_B = N$ and $\phi_A = \phi_B = {}^1/_2$, which was roughly satisfied in the present case, M_D predicted by the fast theory becomes consistent with that by the slow theory. In the present theoretical work, we used the slow theory, because the mean-field theory is consistent with the incompressible assumption, which leads to the slow one.
(34) Pecora, R. *Dynamic Light Scattering*; Prenum Press: New York and London, 1985.
(35) Miyashita, N.; Nose, T. *J. Chem. Phys.* **1994**, *100*, 6028.
(36) Dunbar, J.; North, A. M.; Pethrick, R. A.; Steinheuer, D. B. *J. Polym. Sci., Polym. Phys. Ed.* **1977**, *15*, 263.
(37) Ferry, J. D. *Viscoelastic Properties of Polymers*; Wiley: New York, 1980.
(38) Landry, M. R.; Gu, Q. J.; Yu, H. *Macromolecules* **1988**, *21*, 1158.
(39) von Meerwall, E. D.; Amelar, S.; Smeltzly, M. A.; Lodge, T. P. *Macromolecules* **1989**, *22*, 295.
(40) *International Critical Tables of Numerical Data, Physics, Chemistry and Technology, VOLUME VII*; Washburn, E. W., Ed.; McGraw-Hill Book Co.: New York and London, 1930.
(41) Brown, W.; Zhou, P. *Macromolecules* **1991**, *24*, 1820.

MA950929H